



Supplement of

Absorption enhancement of black carbon particles in a Mediterranean city and countryside: effect of particulate matter chemistry, ageing and trend analysis

Jesús Yus-Díez et al.

Correspondence to: Jesús Yus-Díez (jesus.yus@idaea.csic.es) and Marco Pandolfi (marco.pandolfi@idaea.csic.es)

The copyright of individual parts of the supplement might differ from the article licence.

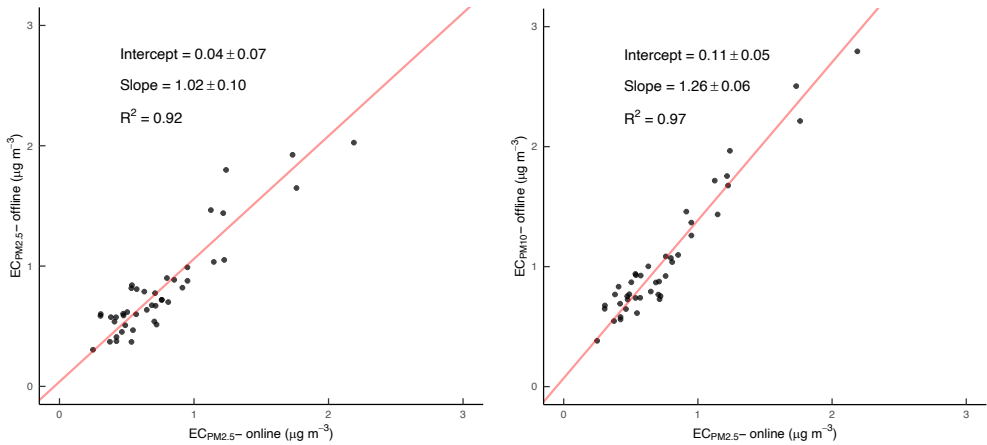


Figure S1: Relationship between the offline 24-hour filter measurements of EC with an inlet cut-off of a) PM2.5 and b) PM10, and the online retrieved measurements of EC with an inlet cut-off of PM2.5.

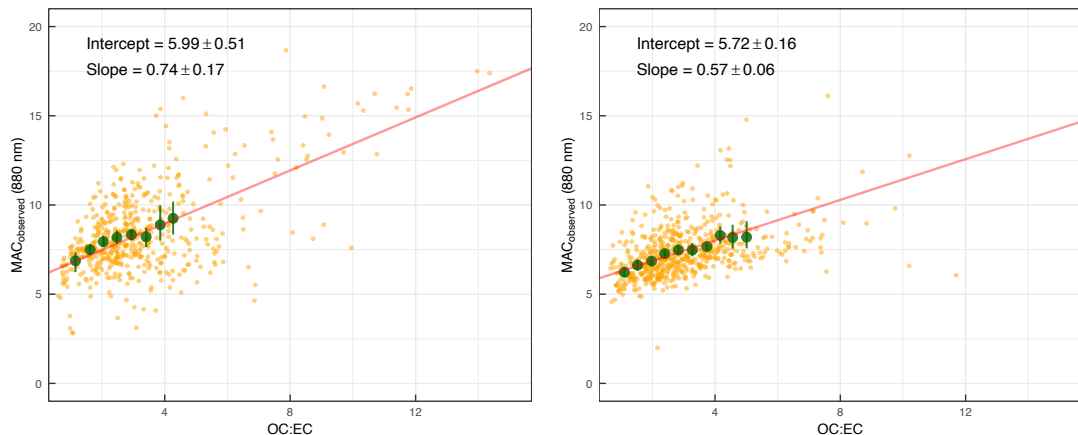


Figure S2: Mass absorption cross-section (MAC) as a function of the online OC-EC ratio at BCN for the AE33 absorption measurement at 880 nm for the a) cold and b) warm period. The intercept obtained with the Deming regression yields the experimental reference MAC of Fig. S3.

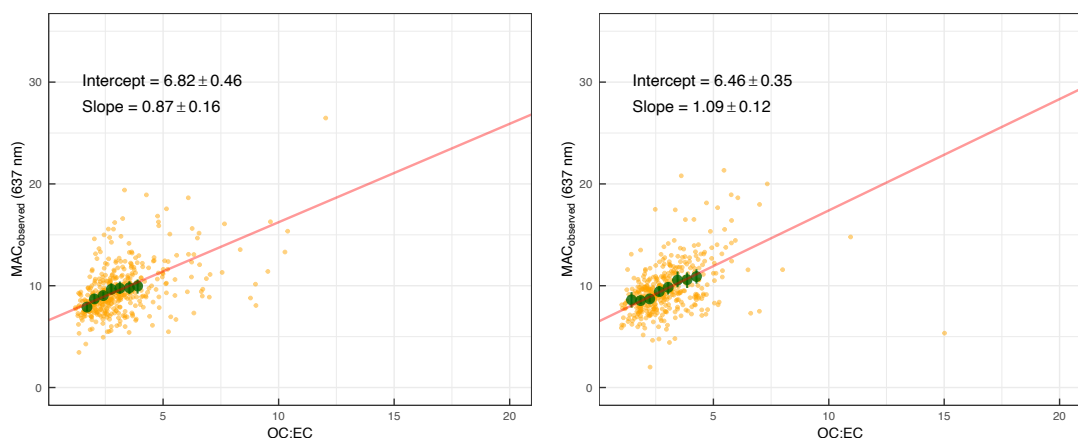


Figure S3: Mass absorption cross-section (MAC) as a function of the offline OC-EC ratio at BCN for the MAAP absorption measurement at 637 nm for the a) cold and b) warm period. The intercept obtained with the Deming regression yields the experimental reference MAC of Fig. S3.

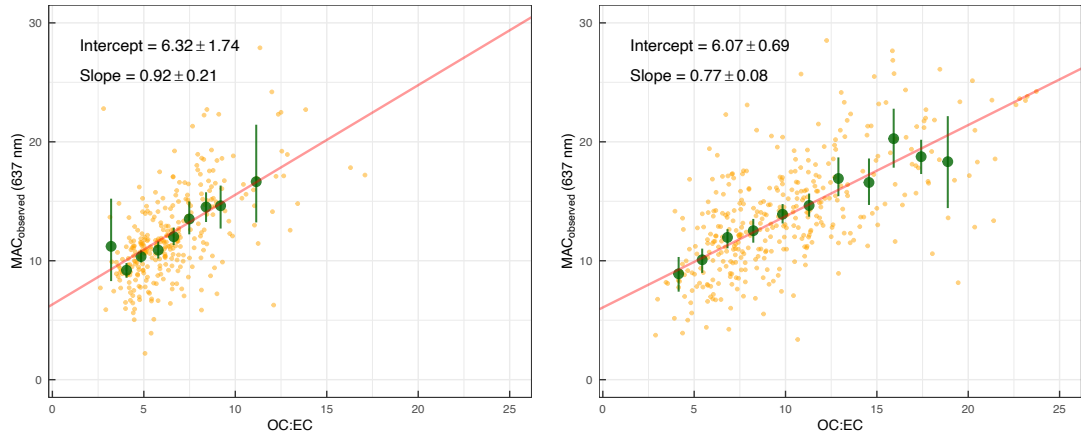


Figure S4: Mass absorption cross-section (MAC) as a function of the offline OC-EC ratio at MSY for the MAAP absorption measurement at 637 nm for the a) cold and b) warm period. The intercept obtained with the Deming regression yields the experimental reference MAC of Fig. S3.

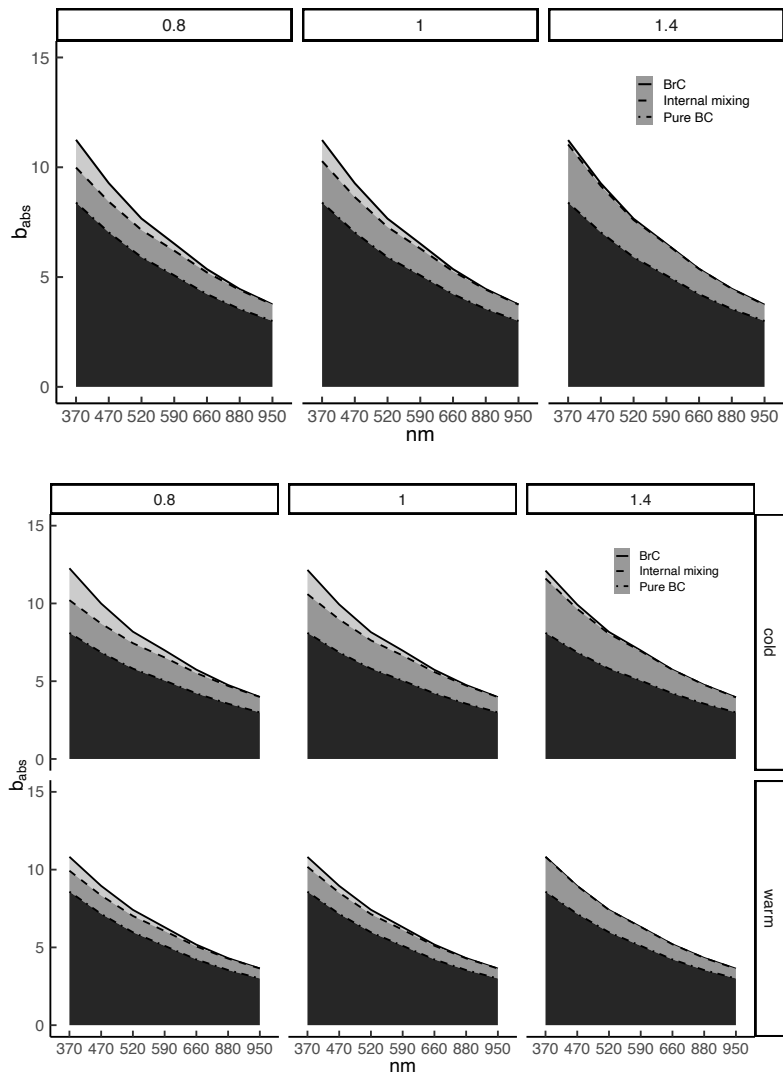


Figure S5: Absorption coefficients, b_{abs} , attribution to both internal and external mixing for the overall measurement period, as well as the cold and warm period under different AAE conditions for the internally mixed BC (0.8, 1, 1.4) for the online measurements at the 7-AE33 wavelengths at Barcelona (BCN).

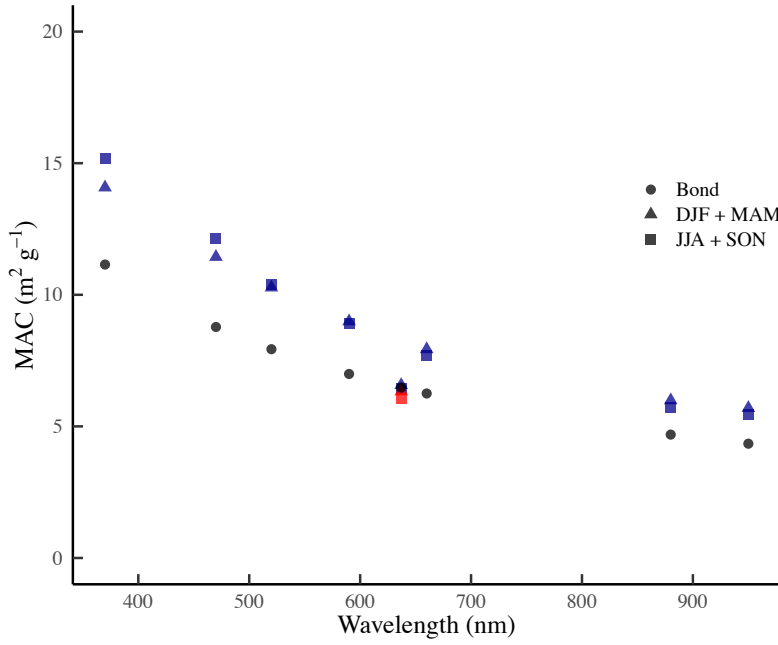


Figure S6: Pure BC MAC ($\text{m}^2 \text{g}^{-1}$) values obtained from Bond et al. (2006), and experimentally from online techniques via AE33 and Sunset online OC:EC measurements at BCN, and offline via a MAAP at 637 nm and offline OC:EC measurements. BCN station is represented by blue points and Montseny by green points.

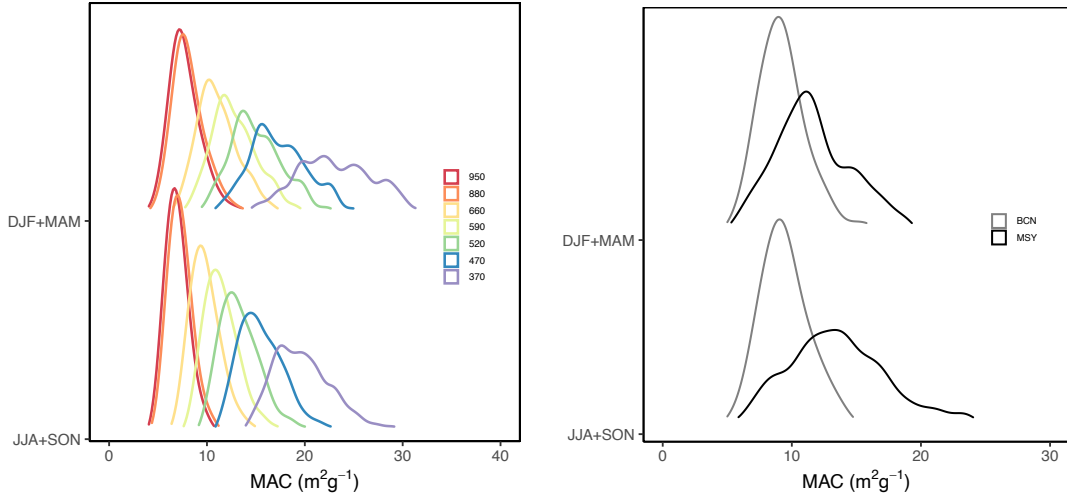


Figure S7: Seasonal frequency distributions of the mass absorption cross-section (MAC) at a) BCN station using a multi-wavelength AE33, and b) at both BCN and MSY at 637 nm using a MAAP.

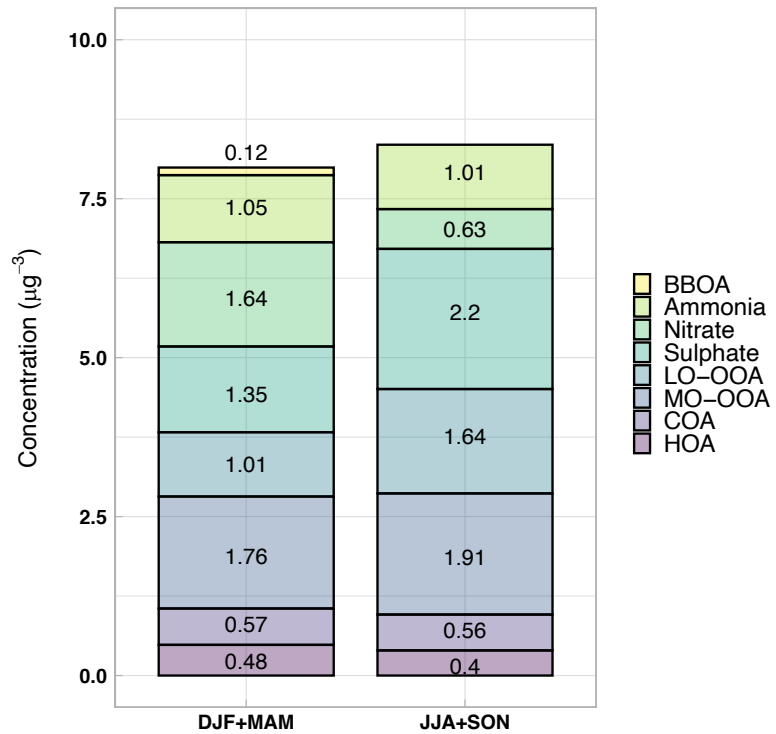


Figure S8: Proportion of the different sources of both organic and inorganic aerosols BCN through-out the seasons during the 2018-2019 period (Via et al., 2021).

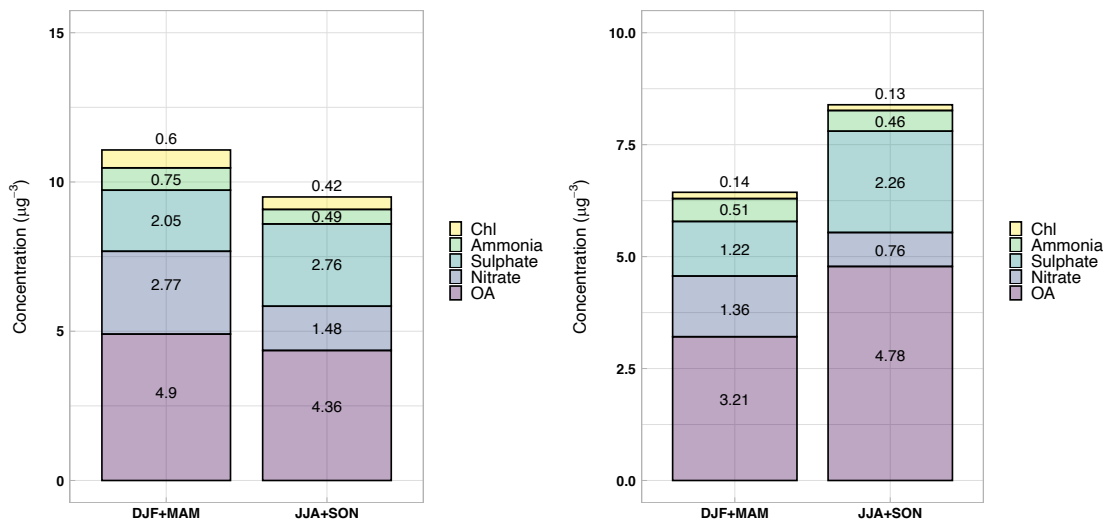


Figure S9: Proportion of the different sources of both organic and inorganic aerosols during the different seasons of the 2011-2018 measurement period at a) BCN, and b) MSY (Veld et al., 2021).

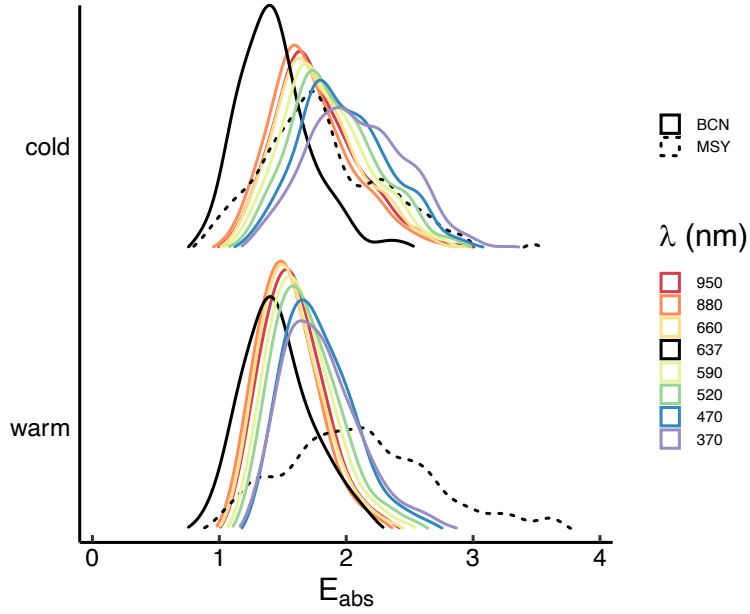


Figure S10: Seasonal frequency distributions of E_{abs} using as a reference MAC the theoretical value provided by Bond et al. (2006) extrapolated to 7 wavelengths measured AE33 wavelengths (370, 470, 520, 590, 660, 880 and 950 nm) at BCN station, and to the MAAP wavelength at 637 nm at both BCN and MSY.

Table S1: Absorption enhancement for both external ($E_{\text{abs,ext}}$) and internal ($E_{\text{abs,int}}$) mixing for the overall period, and the cold and warm period using the experimental MAC ref value.

Overall

AAE	λ (nm)	$E_{\text{abs,int}}$	$E_{\text{abs,ext}}$	% $E_{\text{abs,int}}$	% $E_{\text{abs,ext}}$
0.8					
	370	1.203 ± 0.269	0.245 ± 0.272	83.06	16.94
	470	1.211 ± 0.280	0.171 ± 0.170	87.62	12.38
	520	1.225 ± 0.294	0.133 ± 0.129	90.21	9.79
	590	1.236 ± 0.309	0.101 ± 0.092	92.44	7.56
	660	1.247 ± 0.324	0.069 ± 0.066	94.78	5.22
	880	1.284 ± 0.354	-	100	0
	950	1.284 ± 0.355	-	100	0
1					
	370	1.241 ± 0.320	0.201 ± 0.241	86.07	13.93
	470	1.239 ± 0.317	0.146 ± 0.146	89.47	10.53
	520	1.250 ± 0.327	0.110 ± 0.107	91.88	8.12
	590	1.255 ± 0.334	0.082 ± 0.075	93.84	6.16
	660	1.261 ± 0.343	0.055 ± 0.054	95.83	4.17
	880	1.284 ± 0.354	-	100	0
	950	1.284 ± 0.355	-	100	0
1.4					
	370	1.341 ± 0.453	0.093 ± 0.200	93.51	6.49
	470	1.307 ± 0.407	0.074 ± 0.119	94.61	5.39
	520	1.308 ± 0.403	0.051 ± 0.088	96.28	3.72
	590	1.300 ± 0.392	0.037 ± 0.064	97.23	2.77
	660	1.293 ± 0.385	0.023 ± 0.049	98.25	1.75
	880	1.284 ± 0.354	-	100	0
	950	1.284 ± 0.355	-	100	0

Cold period

AAE	λ (nm)	$E_{abs,int}$	$E_{abs,ext}$	% $E_{abs,int}$	% $E_{abs,ext}$
0.8					
	370	1.231 ± 0.324	0.420 ± 0.268	74.56	25.44
	470	1.240 ± 0.336	0.283 ± 0.165	81.40	18.60
	520	1.250 ± 0.351	0.211 ± 0.126	85.58	14.42
	590	1.262 ± 0.368	0.158 ± 0.093	88.90	11.10
	660	1.274 ± 0.385	0.112 ± 0.066	91.91	8.09
	880	1.326 ± 0.420	-	100	0
	950	1.323 ± 0.421	-	100	0
1					
	370	1.275 ± 0.385	0.363 ± 0.225	77.81	22.19
	470	1.272 ± 0.381	0.243 ± 0.128	83.98	16.02
	520	1.278 ± 0.390	0.182 ± 0.095	87.55	12.45
	590	1.284 ± 0.398	0.132 ± 0.068	90.65	9.35
	660	1.290 ± 0.407	0.093 ± 0.049	93.27	6.73
	880	1.326 ± 0.420	-	100	0
	950	1.323 ± 0.421	-	100	0
1.4					
	370	1.388 ± 0.545	0.217 ± 0.172	86.50	13.50
	470	1.349 ± 0.490	0.148 ± 0.085	90.09	9.91
	520	1.343 ± 0.481	0.106 ± 0.066	92.72	7.28
	590	1.333 ± 0.468	0.075 ± 0.050	94.65	5.35
	660	1.326 ± 0.457	0.053 ± 0.041	96.17	3.83
	880	1.326 ± 0.420	-	100	0
	950	1.323 ± 0.421	-	100	0

Warm period

AAE	λ (nm)	$E_{abs,int}$	$E_{abs,ext}$	% $E_{abs,int}$	% $E_{abs,ext}$
0.8					
	370	1.182 ± 0.202	0.120 ± 0.186	90.75	9.25
	470	1.189 ± 0.210	0.088 ± 0.109	93.08	6.92
	520	1.203 ± 0.226	0.073 ± 0.086	94.31	5.69
	590	1.214 ± 0.238	0.058 ± 0.061	95.42	4.58
	660	1.227 ± 0.253	0.037 ± 0.040	97.10	2.90
	880	1.249 ± 0.271	-	100	0
	950	1.251 ± 0.271	-	100	0
1					
	370	1.216 ± 0.240	0.088 ± 0.166	93.24	6.76
	470	1.215 ± 0.238	0.065 ± 0.095	94.93	5.07
	520	1.226 ± 0.251	0.052 ± 0.072	95.94	4.06
	590	1.232 ± 0.258	0.041 ± 0.050	96.77	3.23
	660	1.241 ± 0.268	0.026 ± 0.032	97.95	2.05

880	1.249 ± 0.271	-	100	0
950	1.251 ± 0.271	-	100	0
1.4				
370	1.305 ± 0.339	0.012 ± 0.153	99.05	0.95
470	1.276 ± 0.306	0.011 ± 0.092	99.16	0.84
520	1.279 ± 0.310	0.004 ± 0.069	99.69	0.31
590	1.272 ± 0.302	0.005 ± 0.051	99.65	0.35
660	1.270 ± 0.300	-0.001 ± 0.037	100.086	-0.086
880	1.249 ± 0.271	-	100	0
950	1.251 ± 0.271	-	100	0

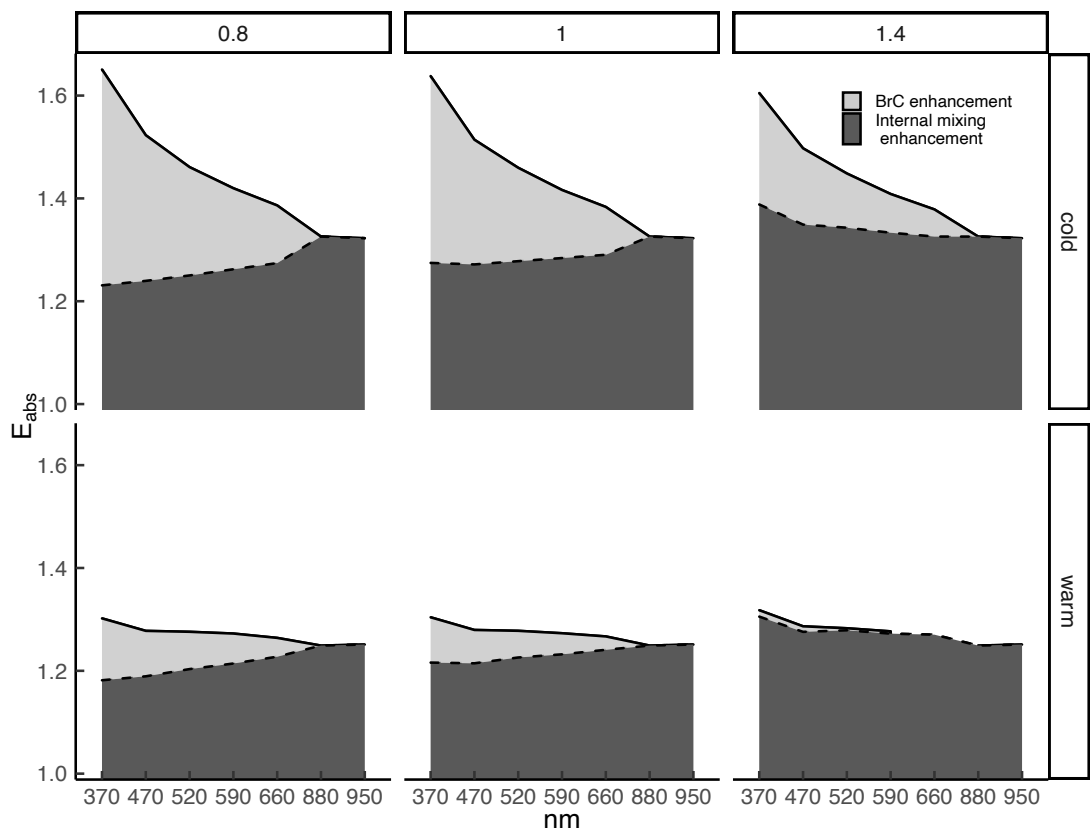


Figure S11: Absorption enhancement, E_{abs} , attribution to both internal and external mixing for both the cold and warm period under different AAE conditions for the internally mixed BC (0.8,1,1.4) for the online measurements at the 7-AE33 wavelengths at Barcelona (BCN).

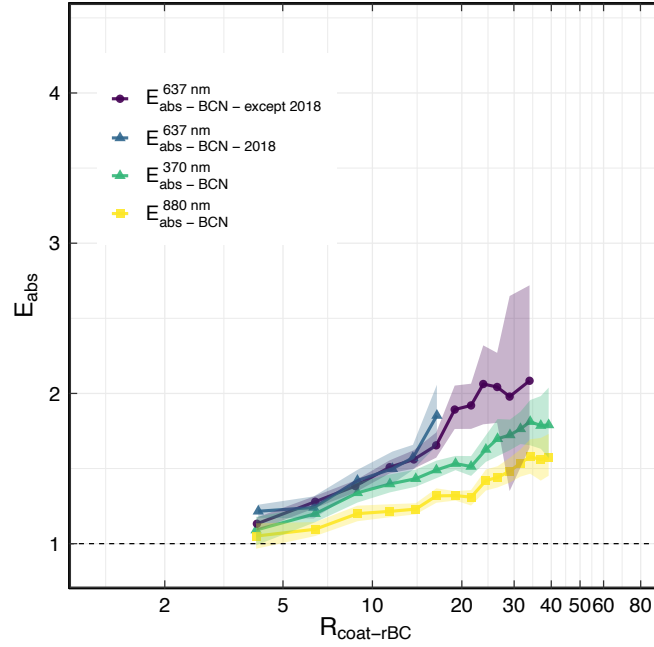


Figure S12: Absorption enhancement, E_{abs} , as a function of the non-refractory PM to EC ratio at BCN station. As in Fig. 3 but omitting the E_{abs} for MSY and showing the values of E_{abs} obtained offline for the MAAP just for 2018 and for all the years except 2018; showcasing the large inter-annual variability.

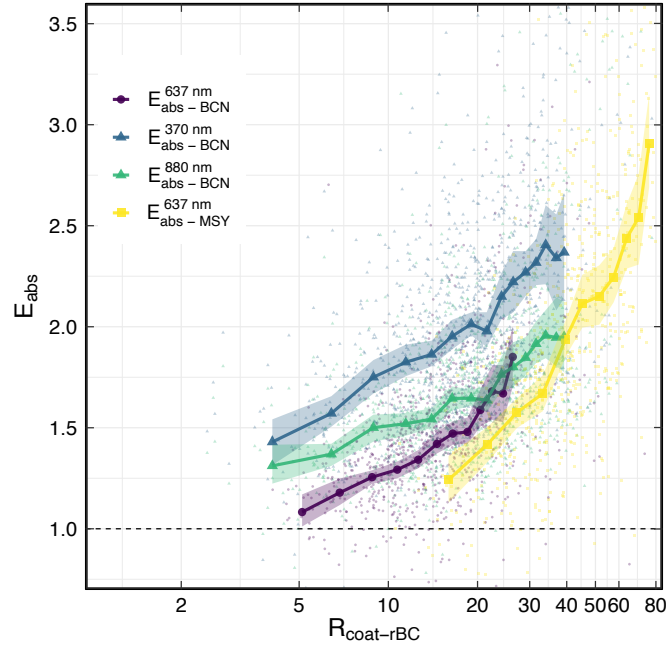


Figure S13: Absorption enhancement, E_{abs} , as a function of the non-refractory PM to EC ratio for BCN and MSY station. As in Fig. 3 but using as a reference MAC the theoretical value provided by Bond et al. (2006) and extrapolating to 370 and 880 nm for the AE33 and online OC:EC and to 637 nm for the MAAP and offline OC:EC.

Table S2: VIF (Variance Inflation Factor) between the independent variables of the multi-linear regression analysis, i.e. the chemical species obtained with the Q-ACSM, and a test of the statistical significance using the p-value of each coefficient (*: $p < 0.05$, **: $p < 0.01$, ***: $p < 0.001$).

	Cold period		Warm period	
	VIF	p-value	VIF	p-value
Intercept	-	***	-	***
HOA-to-EC	1.405	*	1.132	*
BBOA-to-EC	2.247	**	-	-
MO.OOA-to-EC	6.045	*	3.015	
LO.OOA-to-EC	1.385	*	1.827	
SO4-to-EC	2.215		1.913	*
NO3-to-EC	3.315		1.207	***
COA-to-EC	1.179	**	1.515	*

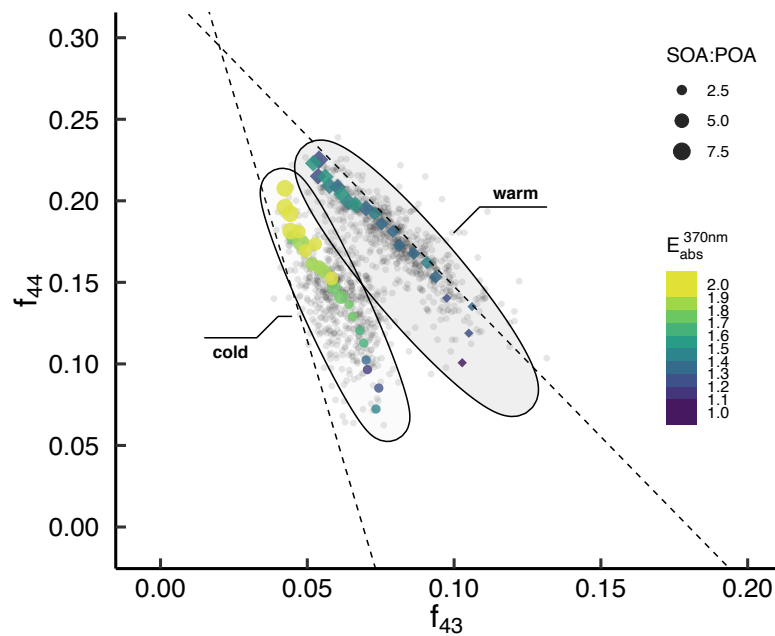


Fig. S14: Absorption enhancement, E_{abs} , at 370 nm at BCN using online measurements as a function of the primary to secondary organic aerosol ratio (POA/SOA), and the atmospheric aging (following Ng. et al., 2010 proposed triangle plot, f_{44} vs f_{43}). The f_{44} and f_{43} factors used are the ones presented by Via et al. (2021) for the same time period from the Q-ACSM measurements.

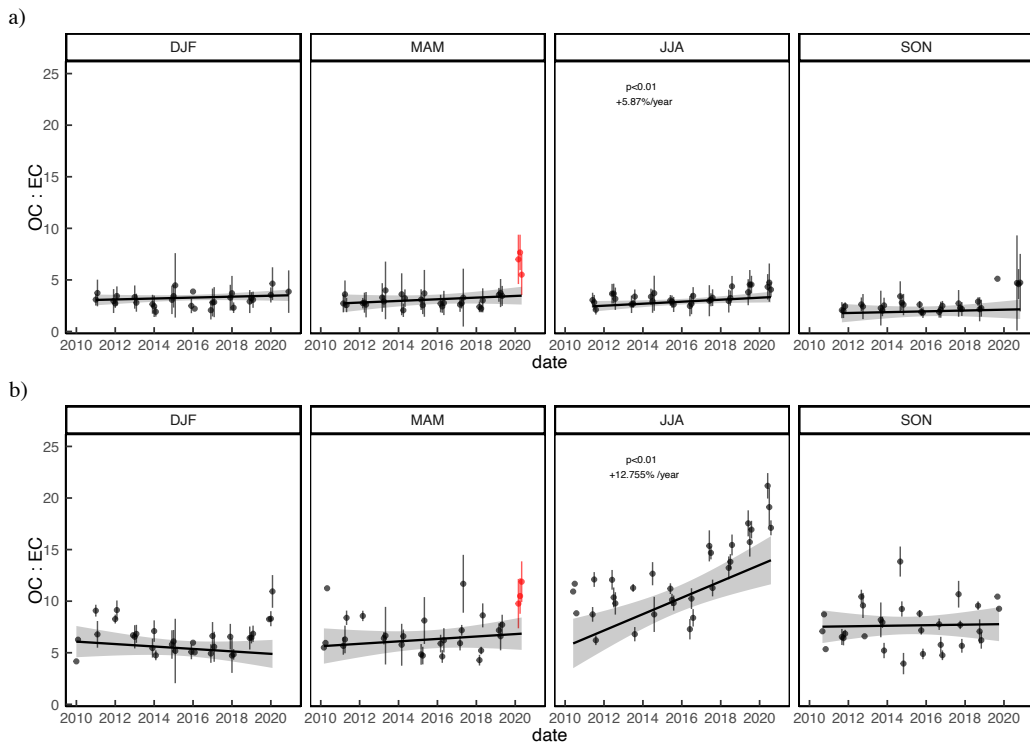


Fig. S15: Seasonal trends of the OC-EC ratio in a) BCN between 2011 and 2020, and b) MSY between 2010 and 2020. COVID-19 lockdown period is marked by the red dots.

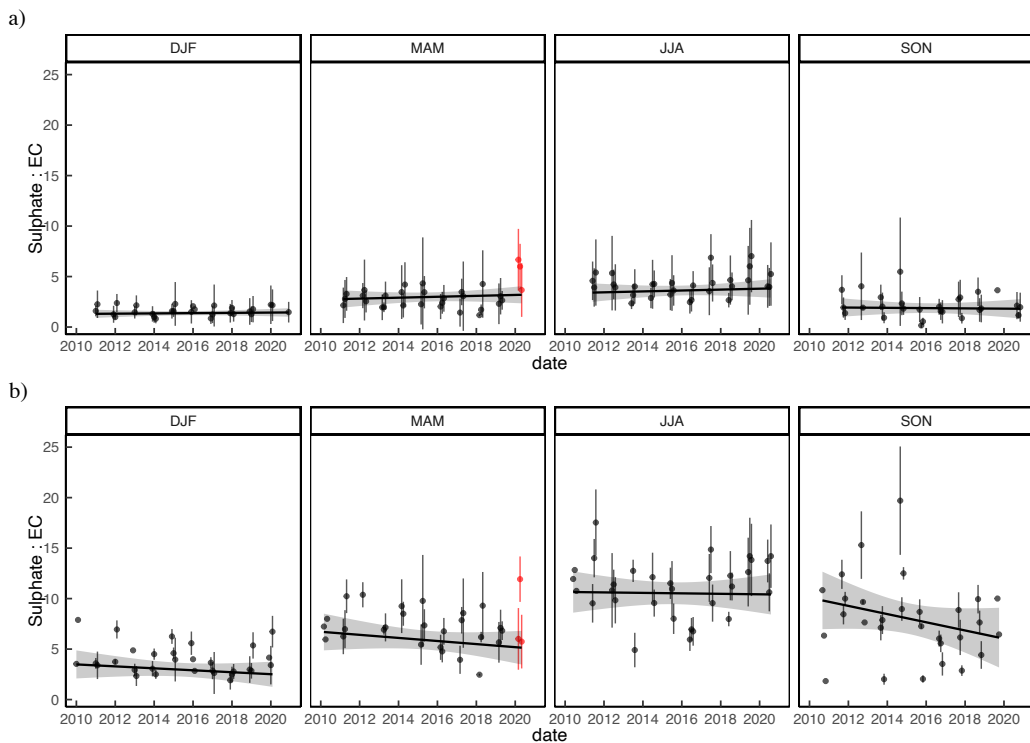


Fig. S16: Seasonal trends of the Sulphate-EC ratio in a) BCN between 2011 and 2020, and b) MSY between 2010 and 2020. COVID-19 lockdown period is marked by the red dots.

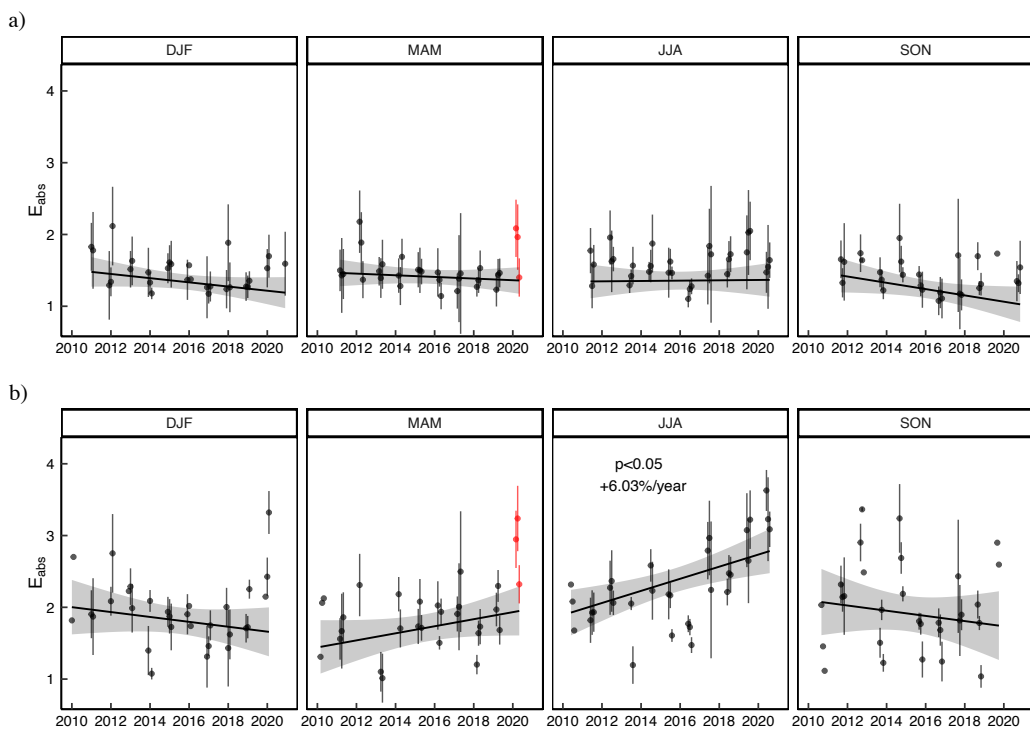


Fig. S17: Absorption enhancement, E_{abs} at 637 nm seasonal trend analysis between 2011 and 2020 at a) Barcelona and b) Montseny station. The trend analysis was performed using a Theil-Sen function over the E_{abs} offline measurements using a theoretical reference MAC (Bond et al., 2006). Dust influenced measurements were excluded. COVID-19 lockdown period is marked by the red dots.